KSCE Journal of Civil Engineering
DOI 10.1007/s12205-024-1698-8

pISSN 1226-7988, eISSN 1976-3808
www.springer.com/12205

Geotechnical Engineering

Heat-water-stress Coupling Model for Saturated Frozen Soil under Different Stress Levels

Zhiming Li[a], **Rui Jiang**[a], **Aiping Tang**[b], **and Rui Zhu**[c]

[a]*School of Architecture and Civil Engineering, Heilongjiang University of Science and Technology, Heilongjiang, Harbin 150022, China*
[b]*School of Civil Engineering, Harbin Institute of Technology, Heilongjiang, Harbin 150090, China*
[c]*School of Transportation Engineering, Nanjing Tech University, Jiangsu, Nanjing 211816, China*

ARTICLE HISTORY

Received 12 August 2023
Revised 16 April 2024
Accepted 17 June 2024
Published Online 03 August 2024

KEYWORDS

Water distribution
Coupling model
Confining pressure
Deviator pressure
Frost heave

ABSTRACT

Ground deformation induced by frost heave is a matter of concern in cold region engineering construction since it affects surrounding structures. Frost heave, which is related to the heat-water-stress interaction, is a complicated process. In this study, a heat-water-stress coupling model was established for saturated frozen soil under different stress levels to quantify the water redistribution, heat transfer, frost heave, and water intake. An empirical formula for the soil permeability considering the confining and deviator pressures was employed as an indispensable hydraulic equation in the coupling model. The Drucker–Prager yield criterion matched with the Mohr–Coulomb criterion was employed in the force equilibrium equation to investigate the deformation due to the deviator and confining pressures. The anisotropic frost heave during unidirectional freezing was further considered in the coupling model by introducing an anisotropic coefficient. Subsequently, based on the above coupling relationship, a mathematical module in COMSOL Multiphysics was applied to calculate the governing equation numerically. Finally, the proposed model was validated through an existing frost heave experiment conducted under various temperature gradients and stress levels. The results of the freezing front, water redistribution, water intake, and frost heave ratio predicted using the proposed model were found to be consistent with the experimental results.

1. Introduction

Infrastructure built in cold regions, such as expressways, railways, tunnels, pipelines, and canals, are more or less facing the deleterious deformation brought by frost heave due to water migration (Azmatch et al., 2012). This deformation, which has a negative influence on surrounding structures, increases the construction cost and period of engineering projects, even threatening their safety. Saturated soil, due to its higher water content and sufficient water supplement, will produce considerable frost heave once the rapid separation of soil particles occurs, which is worthier of scholars' attention. Although a series of anti-frost heave measures have been successfully employed in engineering, understanding the underlying mechanism to predict frost heave under complex geological conditions should be the direction of future research.

Frost heave can be identified as a combination of pristine frost heave (9%), which is due to the transformation of ice/water, and segregated frost heave (109%), which is induced by the freezing of migrated water (Zhang et al., 2018). Therefore, the phenomenon of water migration is the main cause of frost heave; however, this was not recognized until Taber (Taber, 1929, 1930), who observed frost heave by replacing distilled water with a frozen shrinking substance, "benzene." Later, researchers investigated the factors affecting water migration in frozen soil, including the temperature gradient, initial water content, water supply conditions, external load, salt content, and soil mineral composition (Zhang et al., 2017a; 2017b; 2021; Gao et al., 2018; She et al., 2018; Qu et al., 2020; Li et al., 2021; Xue et al., 2021; Zhao et al., 2021). However, the most above experiments were conducted based on the complete lateral restriction. Although it has been confirmed that the horizontal restraint has great influence on the vertical frost heave, few literatures studied the effect of confining pressure on water migration (Lu et al., 2021). Based on the author's limited knowledge, Lu et al. (2021) pioneered to conduct a frost heave

CORRESPONDENCE Zhiming Li lzm_usth@126.com School of Architecture and Civil Engineering, Heilongjiang University of Science and Technology, Heilongjiang, Harbin 150022, China

experiment on saturated clay soil under different stress levels, analyzing the effect of the confining pressure on the frost heave, water content at the freezing front, and quantity of water intake, providing valuable test results for validating the coupling model.

Frost heave is a complicated process, related to the mass transfer, heat transfer, phase transition, and moving boundary. This phenomenon can be described using the multiphysical coupling theory. Coupling models have been studied for more than half a century. Accordingly, many empirical, theoretical, and numerical models have been proposed to describe frost heave. The coupling model, starting from the mechanism of frost heave and focusing on the conditions of frost heave, is the theoretical basis for the investigation and prediction of frost heave. Based on the various assumptions, theoretical basis, formation conditions of ice lens, the driving force of water migration, and independent variables of field equations, a large number of competitive coupling models were deduced for nearly 60 years, such as capillary bundle model (Everett, 1961), hydrodynamic model (Harlan, 1973), segregation potential model (Konrad and Morgenstern, 1981), thermodynamics model (Duquennoi and Fremond, 1989), rigid ice model (O'neill and Miller, 1985), and crystallization kinetics model (Wu et al., 2017). Some other models considering the coupling of the temperature, moisture, salt, stress, and strain have also been proposed (Liu and Yu, 2011; Tan et al., 2011; Li et al., 2017; Yu et al., 2018; Bai et al., 2020; 2022; Ji et al., 2021). Although the variation of the temperature, water distribution, and frost heave can be calculated accurately by these models, the effect of external load on water migration was not considered in these coupling models.

To address this limitation mentioned above, the relationship between the ice, water pressure, and external load in Clapeyron equation for saturated soil were employed (Zhou and Li, 2012; Lai et al., 2014). In their models, the driving force of water migration depended on the external load and further affected the frost heave. Similar method considering external load can be also applied in unsaturated frozen soil by introducing a coefficient of the reduced suction in Clapeyron equation (Yin et al., 2018; Teng et al., 2020; Li et al., 2021). From the point of view of the segregation potential model, Konard and Morgensten (1982) introduced two empirical parameters related to the external load to describe the variation of frost heave. Besides, the external loads can be also considered as part of the matric suction to predict the quantity of the water intake (Ming and Li, 2016), however, the water distribution and frost heave could not be calculated using this model. Recent studies have confirmed that in addition to the external load, the confining pressure has a significant effect on the development of frost heave (Shen et al., 2020). However, few studies have considered this factor in the coupling models. Moreover, some other coupling models are complicated, and the parameters are difficult to determine accurately, which may hinder their wide application in engineering.

The objective of this paper is to develop a new and simple coupled model for saturated frozen soil under different stress levels, to obtain the process of heat transfer, total water redistribution, frost heave, and water intake under different stress levels and temperature gradients. The Drucker–Prager yield criterion, anisotropic frost heave, and an empirical formula for soil permeability considering the pressure were employed in the coupling model to clarify the freezing process accurately. Research on frost heave of saturated frozen soil in this paper helped confirm that the proposed model can serve as a reference for controlling frost heave of in cold-saturated regions.

2. Heat-water-stress Coupling Model for Saturated Frozen Soil

Figure 1 shows the schematic of the ice, unfrozen water, and soil grain in saturated frozen soil. Due to the capillarity and surface energy of the soil particles, some amount of water remains unfrozen and attached to the surface of the particles when the temperature reaches the freezing point (Li et al., 2020). In the figure, S_i is the ice ratio, that is, the ratio of the ice content to the porosity n. The porosity n is constantly varying with the freezing process. Therefore, the content of each phase can be expressed as:

$$\theta_s = 1-n,\ \theta_i = nS_i,\ \theta_l = n\left(1-S_i\right), \tag{1}$$

where θ_s, θ_i, and θ_l are the volumetric content of the soil grain, ice, and unfrozen water content, respectively.

The ice ratio can be empirically expressed as a function of the temperature (Li et al., 2017):

$$S_i = \begin{cases} 1-\left[1-\left(T-T_f\right)\right]^a, & T \le T_f \\ 0, & T > T_f \end{cases} \tag{2}$$

where T and T_f are the temperature and freezing point of the soil, respectively; a is the freezing coefficient related to the Soil Freezing Characteristic Curve (SFCC).

2.1 Basic Assumption

To simplify the coupling mechanism of the heat-water-stress in saturated frozen soil, the following five assumptions are first made:

1. Because of the small variation range of deviatoric and

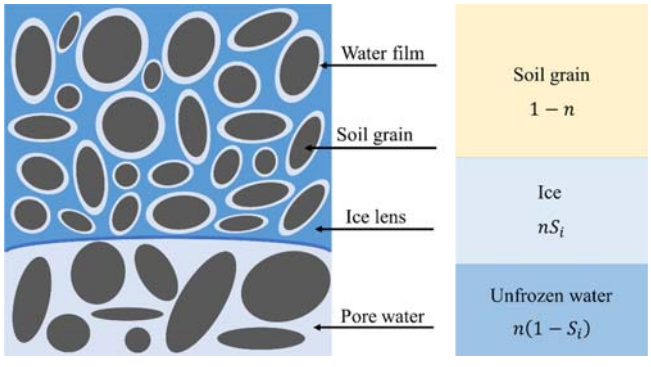

Fig. 1. Schematic of Ice, Unfrozen Water, and Soil Grain in Saturated Frozen Soil

confining pressure in the experiment, the freezing point drop is ignored.
2. Water migration obeys Darcy's law.
3. The effect of vapor migration on frost heave is ignored.
4. Heat losses through insulated walls can be neglected in a numerical simulation.
5. The elastoplastic constitutive relation of soil is considered.
6. The water content in the unfrozen zone for the open system is equal to the initial water content.

2.2 Coupling Equation of Temperature and Hydraulic Field

Based on the principle of energy conservation and Fourier's law, the governing equation for the temperature field considering the ice/water transformation and water convection in the saturated frozen soil can be expressed as:

$$\rho C\frac{\partial T}{\partial t}=\nabla\cdot(\lambda\nabla T)+L\rho_i\frac{\partial\theta_i}{\partial t}-C_l\rho_l\mathbf{u}\cdot\nabla T, \tag{3}$$

where ρ, ρ_l, and ρ_i represent the densities of the porous media, unfrozen water, and ice, respectively; C and λ denote the specific heat capacity and thermal conductivity of the porous media, respectively; C_l represents the specific heat capacity of the water; L is the latent heat of water/ice transformation; $\mathbf{u}$ (u_x, u_y) is the velocity of the water flow; and t is the time.

The specific heat capacity and thermal conductivity of the porous media can be calculated based on the volume fraction and thermal parameters of each phase, respectively, expressed as:

$$C=(1-n)C_s+nS_iC_i+n(1-S_i)C_l, \tag{4}$$

$$\lambda=\lambda_s^{\,1-n}\lambda_i^{\,nS_i}\lambda_l^{\,n(1-S_i)}, \tag{5}$$

where C_s and C_i are the specific heat capacities of the soil grain and ice, respectively; λ_s, λ_i, and λ_l represent the thermal conductivities of the soil grain, ice, and water, respectively.

Since the horizontal water flow is ignored due to the unidirectional freezing condition, the velocity of the water flow along the direction of heat flow u_y can be calculated based on Darcy's equation:

$$u_y=-k_y\frac{\partial\varphi}{\partial y}, \tag{6}$$

where φ is the matric suction head, and k_y is the soil permeability in the y-direction.

According to the chain rule, Darcy's equation can be expressed as (Lu, 2004):

$$u_y=-k_y\frac{\partial\varphi}{\partial\theta_l}\frac{\partial\theta_l}{\partial y}=-\frac{k_y}{C_\varphi}\frac{\partial\theta_l}{\partial y}=-D\frac{\partial\theta_l}{\partial y}, \tag{7}$$

where C_φ is the specific water capacity, and D is the soil water diffusivity.

When ice forms in a frozen zone, it will impede the movement of water, thereby decreasing the soil water diffusivity. Taking this into account in the model, Darcy's equation can be modified as (Li et al., 2017):

$$u_y=-I\frac{k_y}{C_\varphi}\frac{\partial\theta_l}{\partial y}=-10^{-10\theta_i}\frac{k_y}{C_\varphi}\frac{\partial\theta_l}{\partial y}=D\frac{\partial\theta_l}{\partial y}, \tag{8}$$

where I denotes the impedance coefficient.

The hydraulic field equation considering the gravitational effect can be obtained based on Richards's equation:

$$\frac{\partial\theta_l}{\partial t}+\frac{\rho_i}{\rho_l}\frac{\partial\theta_i}{\partial t}=\nabla\cdot(D\nabla\theta_l)+\frac{\partial k_y}{\partial y}. \tag{9}$$

Substituting Eq. (1) into Eq. (3) and Eq. (9), the coupling equations of the temperature and hydraulic field can be expressed as:

$$\left(\rho C-L\rho_i n\frac{\partial S_i}{\partial T}\right)\frac{\partial T}{\partial t}=\nabla\cdot(\lambda\nabla T)+LS_i\rho_i\frac{\partial n}{\partial t}-C_l\rho_l\mathbf{u}\cdot\nabla T, \tag{10}$$

$$\left(1+\frac{\rho_i}{\rho_l}S_i-S_i\right)\frac{\partial n}{\partial t}-n\frac{\partial S_i}{\partial T}\frac{\partial T}{\partial t}=\nabla\cdot(D\nabla n)-\nabla\cdot(D\nabla nS_i)+\frac{\partial k_y}{\partial y}. \tag{11}$$

The above governing equations provides a coupling framework with the porosity and temperature as the field variables; however, the deviator and confining pressures were not considered in the coupling model. Li et al. (1998) concluded that the soil permeability decreases exponentially with the external load based on experiments, expressed as:

$$k_y'=k_y(q_e)=k_y\exp(-b_1q_e/q_0). \tag{12}$$

As for the influence of confining pressure on soil permeability, Yuan et al. (2012) proved by a series of experiments that the permeability of soil-cement increases exponentially with decreasing confining pressure. By analogy with the soil-cement and Eq. (12), the soil permeability can be assumed to change exponentially with the increase in the confining and deviator pressure, expressed as:

$$k_y'=k_y(q_e,p_e)=k_y\exp(-b_1q_e/q_0)\cdot\exp(-b_2p_e/p_0), \tag{13}$$

where p_e and q_e are the confining and deviator pressures, respectively; b_1 and b_2 are the undetermined parameters related to the soil properties; p_0 and q_0 are the reference pressures, both of which are equal to 1 kPa in this study.

Based on assumption 2, the modified soil water diffusivity D' can be expressed as:

$$D'=-10^{-10\theta_i}\frac{k_y'}{C_\varphi}=\exp(-b_1q_e/q_0)\cdot\exp(-b_2p_e/p_0)D. \tag{14}$$

2.3 Static Balance Equation

The compressive deformation of the frozen soil is generally considered positive in geotechnical engineering. Based on the principle of local equilibrium, the static balance equation can be expressed as (Li et al., 2015):

$$[L]^T\{\sigma\}-\{F\}=\{0\}, \tag{15}$$

where $[L]$ is the differential operator matrix, $[L] = [\partial/\partial x, 0, \partial/\partial y; 0, \partial/\partial y, \partial/\partial x]^T$; $\{\sigma\}$ is the total stress vector, $\{\sigma\} = \{\sigma_x, \sigma_y, \tau_{xy}\}^T$; $\{F\}$ represents the external force vector, $\{F\} = \{F_x, F_y\}^T$.

The displacement of the frozen soil can be calculated from the strain–displacement relationship, expressed as:

$$[L]\{u\} + \{\varepsilon\} = \{0\}, \tag{16}$$

where $\{u\}$ is the displacement vector, $\{u\} = \{u_x, u_y\}^T$; $\{\varepsilon\}$ is the strain vector, $\{\varepsilon\} = \{\varepsilon_x, \varepsilon_y, \varepsilon_{xy}\}^T$.

When the deviator and confining pressures act on the surface of the frozen soil column, the constitutive model considering the plastic strain and frost heave strain can be written as (Shen and Branko, 1987):

$$[D_T]\left(\{\Delta\varepsilon\} - \{\Delta\varepsilon_v\} - \{\Delta\varepsilon_p\}\right) = \{\Delta\sigma\}, \tag{17}$$

where $[D_T]$ is the elastic matrix, which depends on the temperature, and a detailed description can be found in Appendix; $\{\Delta\varepsilon\}$, $\{\Delta\varepsilon_v\}$, and $\{\Delta\varepsilon_p\}$ represent the total strain increment vector, volumetric strain increment vector induced by frost heave, and plastic strain increment vector, respectively; $\{\Delta\sigma\}$ is the stress increment vector.

The plastic strain increment vector can be calculated based on the assumption of the associated flow law:

$$\{\Delta\varepsilon_p\} = \mathrm{d}\lambda \frac{\partial F}{\partial\{\sigma\}}, \tag{18}$$

where $\mathrm{d}\lambda$ is the plastic scalar factor; F is the yield function, which can be calculated based on the Drucker–Prager yield criterion matched with the Mohr–Coulomb criterion.

The total volumetric strain increment induced by frost heave for conventionally unidirectional freezing test can be expressed as (Zhou and Li, 2012):

$$\Delta\varepsilon_v = \frac{\Delta e}{1+e_0} = \frac{\Delta n}{1-n}, \tag{19}$$

where Δe and Δn are the increments in the void ratio and porosity, respectively; e_0 is the initial void ratio.

The frost heave can be obtained by integrating the above strain along the height:

$$H = \int_0^{H_t} \Delta\varepsilon_v \mathrm{d}y = \int_0^{H_t} \frac{\Delta e}{1+e_0}\mathrm{d}y = \int_0^{H_t} \frac{\Delta n}{1-n}\mathrm{d}y. \tag{20}$$

Here, H is the frost heave with the lateral confinement; H_t is the frozen depth of the soil column at time t.

In this study, the lateral side of the frozen soil column is allowed to deform, since there is no deformation limitation on the sides. Shen and Branko (1987) assumed that both frozen and unfrozen soils are isotropic. Hence, the strain due to frost heave in each direction can be expressed as:

$$\{\Delta\varepsilon_v\} = \left\{\Delta\varepsilon_v^x, \Delta\varepsilon_v^y, \Delta\varepsilon_v^z\right\} = \left\{\frac{1}{3}\Delta\varepsilon_v, \frac{1}{3}\Delta\varepsilon_v, \frac{1}{3}\Delta\varepsilon_v\right\}. \tag{21}$$

However, layers of freezing fronts are formed perpendicular to the heat flow direction during the freezing process. With the variation in the freezing temperature, the freezing front also develops in parallel, indicating that the mechanical properties of the frozen soil along the freezing front and the heat flow direction are quite different (Cai et al., 2015). In this condition, the deformation induced by the frost heave of the frozen soil should be anisotropic: the main direction is along the heat flow direction, the other two main directions are perpendicular to the heat flow direction, and frost heave mainly occurs along the heat flow direction.

Considering the anisotropic nature of the frost heave, a modified function g is employed to reflect this anisotropic property, and the strain caused by frost heave in each direction can be expressed as:

$$\{\Delta\varepsilon_v\} = \left\{\Delta\varepsilon_v^x, \Delta\varepsilon_v^y, \Delta\varepsilon_v^z\right\} = \left\{\frac{1-g}{2}\Delta\varepsilon_v, g\Delta\varepsilon_v, \frac{1-g}{2}\Delta\varepsilon_v\right\}, \tag{22}$$

where the heat flow direction is in the y-direction in this study.

The important point is how to determine the modified function g. The value of this function may be influenced by the confining pressure, deviator pressure, and temperature gradient. By adjusting the value of g under different test conditions, the calculated maximum frost heave was close to the experimental maximum frost heave. Therefore, the modified function g can be written as:

$$g = g\left(T_g, q_e, p_e\right), \tag{23}$$

where T_g is the temperature gradient.

Therefore, the frost heave H' without lateral confinement can be calculated as:

$$H' = g\int_0^t \Delta\varepsilon_v \mathrm{d}y = g\int_0^t \frac{\Delta e}{1+e_0}\mathrm{d}y = g\int_0^t \frac{\Delta n}{1-n}\mathrm{d}y = gH. \tag{24}$$

The transient frost heave ratio η can be calculated as:

$$\eta = \frac{H'}{H_t} \times 100\%. \tag{25}$$

Equations (1) – (25) are fundamental heat-water-stress coupling equations for the saturated frozen soil under different stress levels. The other necessary parameters are provided in Appendix.

3. Numerical Simulation of Soil-column Tests

3.1 Outline

Based on the proposed heat-water-stress coupling model, a numerical simulation was conducted and compared with the corresponding experimental results obtained from a soil column test reported in previous research (Lu et al., 2021).

Lu et al. (2021) conducted a thorough soil column test on a cylindrical soil sample (clay taken from Harbin, China) with a height of 5 cm and a radius of 5 cm in an open system, considering various temperature gradients, confining pressures, and deviator pressures. Initially, the temperature and pressure of the corresponding soil column remained stable before the test; Subsequently, the

warm end, cold end, and initial temperature of the soil column were controlled using three circulated cooling equipment based on the test conditions. A nonpressure water device was used in this test, and the water intake was recorded. Notably, the soil was saturated; however, unfortunately, the value of the saturated water content was not mentioned. For a convenient calculation, the value of the saturated mass water content was set to 0.279. Table 1 presents the test conditions of the open system. The details of the test introduction can be found in the work conducted by Lu et al.

The mathematical module in COMSOL Multiphysics 5.5 was employed to solve the derived equations numerically. The calculated region followed the actual size of soil column. For the thermal boundary condition in the model, Dirichlet temperature boundary conditions on the top and bottom surface of soil were used to control temperatures; Adiabatic boundary condition was applied to the lateral of soil column. For the hydraulic boundary condition, only zero-flux boundary was used on the side of soil column. For the mechanical boundary condition, external loads were exerted on the top and side of soil column, while the bottom of soil was set as fixed. The calculated period and step length were 20 h and 0.1 h, respectively. Table 2 presents the parameters of the frozen soil column used for solving the governing equations. The other calculated parameters can be found in Appendix.

Table 1. Test Conditions of Open System

No.	Top temperature (°C)	Bottom temperature (°C)	Confining pressure (kPa)	Deviator pressure (kPa)
#1	−5.99	1.63	20	1.5
#2	−6.15	1.60	20	23.40
#3	−6.11	1.58	20	40.19
#4	−6.08	1.58	20	60.22
#5	−6.10	0.47	0	41.60
#6	−6.11	0.53	20	40.40
#7	−6.12	0.40	40	40.21
#8	−4.02	1.59	20	41.52
#9	−7.96	1.58	20	40.87

3.2 Parameter Determination

In the proposed coupling model, the most essential procedure is to determine the fitting parameters of the permeability and anisotropic frost heave coefficient under different test conditions. First, the fitting parameters of the permeability is introduced. Lu et al. (2021) did not provide the specific permeability values under different test conditions. Fortunately, the data of the amount of water intake were provided in their study; these can be adopted to determine the permeability given the dependence between the water intake and permeability. The calculated expression of the water intake Q can be written as:

$$Q = \pi\left(r + \frac{1-g}{4}H\right)^2 \int_0^{+H'} (n - n_0)\,\mathrm{d}y\,, \tag{26}$$

where r is the radius of the soil column; n_0 is the initial porosity without freezing.

Based on the principle that the calculated value of the water intake is approximately equal to the experimental value, the permeability can be determined, as listed in Table 3. Fig. 2 shows the calculated and fitting results obtained using Eq. (13) of the soil permeability under different test conditions, in which the fitting parameters b_1 and b_2 in Eq. (13) are equal to 7.535×10^{-3} and 2.488×10^{-3}, respectively.

The anisotropic function g can be determined based on the measured frost heave ratio. When the calculated value of Eq. (24) is consistent with the measured maximum frost heave, the value of g is the anisotropy coefficient used in the model. Table 4 presents the value of g under different test conditions. From the available test data and relevant results, the deviator pressure has

Table 2. Soil Parameters

Parameter	Value/Unit	Parameter	Value
Freezing point T_0	272.35 K	Density of soil grain ρ_s	2,700 kg m^{-3}
Latent heat of water freezing L	334.5 kJ kg^{-1}	Density of water ρ_l	1,000 kg m^{-3}
Permeability of saturated soil k_0	5.215×10^{-9} m s^{-1}	Density of ice ρ_i	917 kg m^{-3}
Gravitational acceleration g	9.8 m s^{-2}	Dry density of soil ρ_d	1,540 kg m^{-3}
Volumetric heat capacity of soil grain C_n	2,160 kJ m^{-3} K^{-1}	Thermal conductivity of soil grain λ_s	1.2 W m^{-1} K^{-1}
Volumetric heat capacity of water C_l	4,180 kJ m^{-3} K^{-1}	Thermal conductivity of water λ_l	0.58 W m^{-1} K^{-1}
Volumetric heat capacity of ice C_i	1,874 kJ m^{-3} K^{-1}	Thermal conductivity of ice λ_i	2.22 W m^{-1} K^{-1}
Freezing coefficient a	−2		

Table 3. Permeability under Different Test Conditions

No.	Permeability (m/s)	No.	Permeability (m/s)	No.	Permeability (m/s)
#1	4.90×10^{-9}	#4	3.12×10^{-9}	#7	3.52×10^{-9}
#2	4.15×10^{-9}	#5	3.84×10^{-9}	#8	3.65×10^{-9}
#3	3.65×10^{-9}	#6	3.65×10^{-9}	#9	3.65×10^{-9}

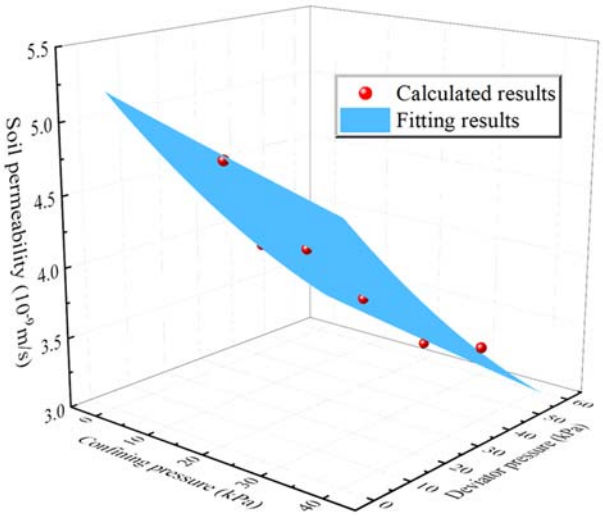

Fig. 2. Calculated and Fitted Results of the Soil Permeability under Different Test Conditions

Table 4. Anisotropic Function g under Different Test Conditions

No.	g	No.	g	No.	g
#1	0.63	#4	0.59	#7	0.82
#2	0.60	#5	0.72	#8	0.41
#3	0.61	#6	0.78	#9	0.77

little effect on the frost heave ratio in the given test results (#1 – #4). The value of g increases linearly with the increase in the confining pressure due to the increase in the lateral constraint (#5 – #7). Moreover, the value of g increases linearly with the increase in the temperature gradient due to the increase in the strength of the frozen soil (#3, #8, and #9). However, because of the difference between the designed test and the real conditions, particularly the fact that the temperatures at the warm and cold ends are difficult to keep constant, it is challenging to propose an empirical formula for g based on the test results.

3.3 Influence of Deviator Pressure on Hydro-thermal-mechanical Performance

Figure 3 shows the total mass water content distribution after freezing for 20 h under different deviator pressures. The water inside the specimens accumulated near the position of the freezing front under the temperature gradient. However, with increasing deviator pressure, the amount of water accumulation gradually decreased. This can be explained by the fact that the increase in the deviator pressure reduces the hydraulic conductivity of the soil and simultaneously restricts the amount of water migration. For the case where the deviator pressure is 1.5 kPa, the maximum total mass water content reaches 115%; however, for the case where the deviator pressure is 60.22 kPa, the maximum total mass water content only reaches 73%. In other words, the deviator pressure has a significant impact on the amount of water migration in frozen soil.

To validate the efficacy of the proposed model, a comparison between the experimental and calculated total mass water contents after freezing for 20 h under different deviator pressures is shown in Fig. 4. The calculated results are in good agreement with the experimental results, particularly the total water content near the freezing front. However, the average mass water content has a certain deviation in the frozen zone in that the calculated value is slightly greater than the experimental one. This may be related to the value of the initial water content, because the initial water content was not provided by Lu et al. (2021). Since the mass water content in the unfrozen zone is assumed to remain constant in our study, the method to determine the initial water content is based on the test water content in the unfrozen zone. In fact, the mass water content in the unfrozen zone also slightly increases after freezing, which may lead to overestimation of the initial water content and then further overestimation of the total water content in the frozen zone. However, overall, the variation trend in the coupling model is consistent with the test value, which is convenient for predicting the water content in cold regions.

Figure 5 shows the dynamic variation in the freezing front and frost heave ratio under different deviator pressures. Fig. 5(a) shows that the variation in the freezing front calculated is consistent with that obtained from the test. Moreover, the variation in the freezing front is consistent under different deviator pressures, and the small deviations may be due to the slight differences in the temperature gradient. Fig. 5(b) shows that the calculated

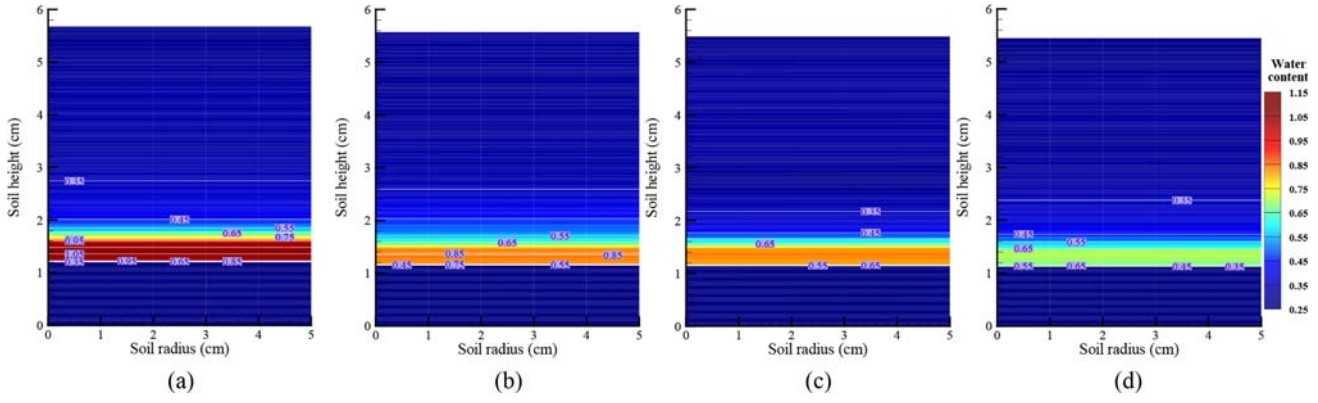

Fig. 3. Distribution of the Total Mass Water Content after Freezing for 20 h under Different Deviator Pressures: (a) #1, (b) #2, (c) #3, (d) #4

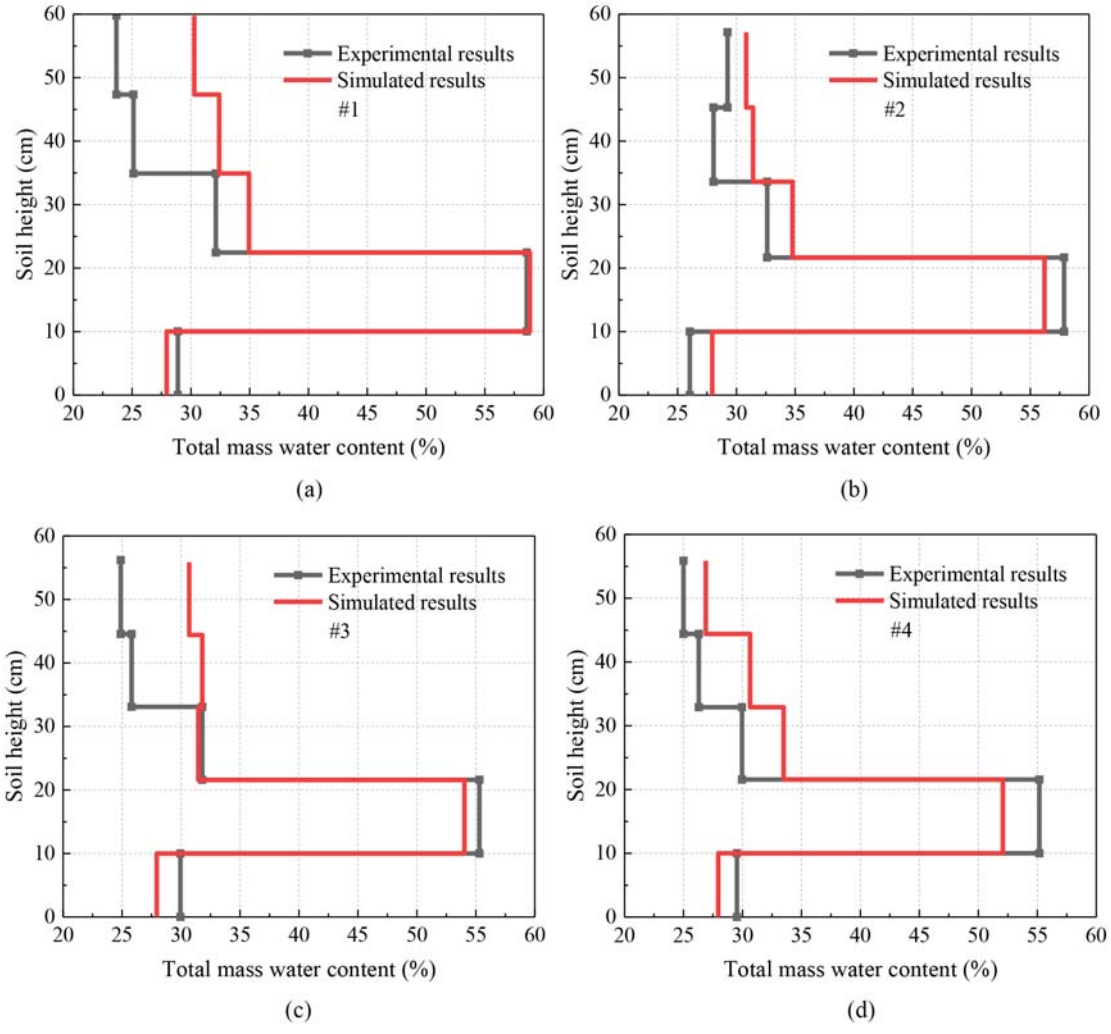

Fig. 4. Comparison between the Experimental and Calculated Total Mass Water Contents after Freezing for 20 h under Different Deviator Pressures: (a) #1, (b) #2, (c) #3, (d) #4

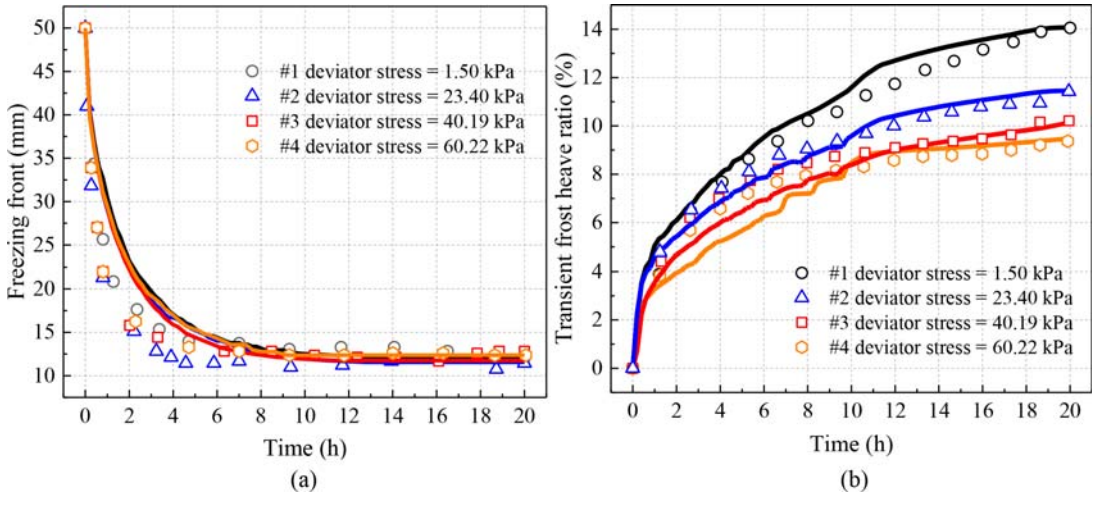

Fig. 5. Dynamic Variation in the Freezing Front and Frost Heave Ratio under Different Deviator Pressures (Symbol: Experimental Results; Line: Calculated Results): (a) Freezing Front, (b) Frost Heave Ratio

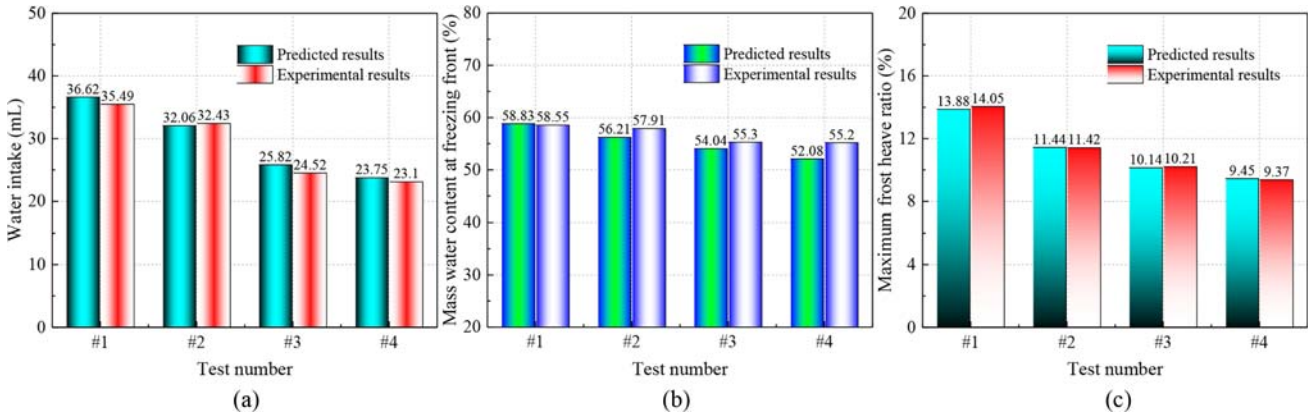

Fig. 6. Comparison between the Calculated and Experimental Results under Different Deviator Pressures: (a) Water Intake, (b) Mass Water Content at the Freezing Front, (c) Maximum Frost Heave Ratio

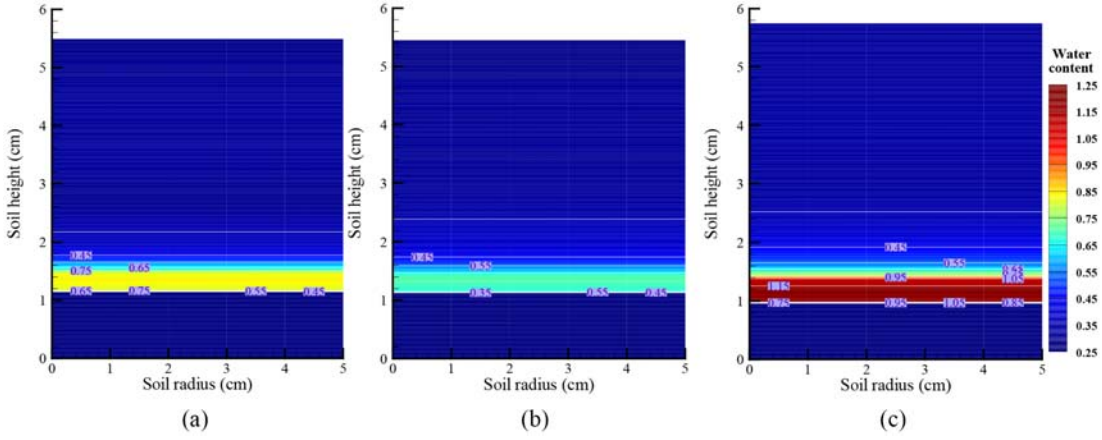

Fig. 7. Total Mass Water Content Distribution after Freezing for 20 h under Different Temperature Gradients: (a) #3, (b) #8, (c) #9

result of the frost heave ratio with time is in good agreement with the experimental result. During the freezing process, the frost heave ratio gradually increased, whereas its rate decreased with time.

To validate the model more intuitively, Fig. 6 shows comparisons of the calculated and experimental results, such as of the water intake, mass water content at the freezing front, and maximum frost heave ratio under different deviator pressures. The experimental and calculated results are highly consistent under different deviator pressures, indicating that the proposed model can be employed to predict the water intake, frost heave, dynamic freezing front, and water redistribution when considering the deviator pressure.

3.4 Influence of Temperature Gradient on Hydro-Thermal-Mechanical Performance

Figure 7 shows the total mass water content distribution after freezing for 20 h under different temperature gradients. The greater the temperature gradient, the greater the amount of water accumulated near the freezing front. This is because the temperature at the warm end is almost similar in the three cases considered; with the increase in the temperature gradient, the temperature at the cold end decreases, and the freezing front is closer to the position of nonpressure water supply; thus, more water accumulates near the freezing front. In addition, because the temperature gradient is high initially, and the water near the cold end does not have sufficient time to migrate, the water content here does not change much.

Figure 8 shows a comparison between the experimental and calculated total mass water contents after freezing for 20 h under different temperature gradients. The proposed model can effectively predict the water redistribution. However, for the case #8, there seems to be a certain deviation in the position of the maximum water content between the calculated and experimental results. This can be attributed to certain errors in determining the position of the freezing fronts in the study by Lu et al. (2021); nevertheless, the calculated maximum mass water content accumulation near the freezing front is consistent with experimental results for case #8.

Figure 9 shows the dynamic variation in the freezing front and frost heave under different temperature gradients. When the temperature at the warm end keeps constant, the depth of the freezing front inside the soil increases with increasing temperature gradient. Meanwhile, the frost heave ratio is also influenced by the temperature gradient due to the difference in the content of water accumulated near the freezing front. Under the condition that the temperature at the warm end is basically the same, the

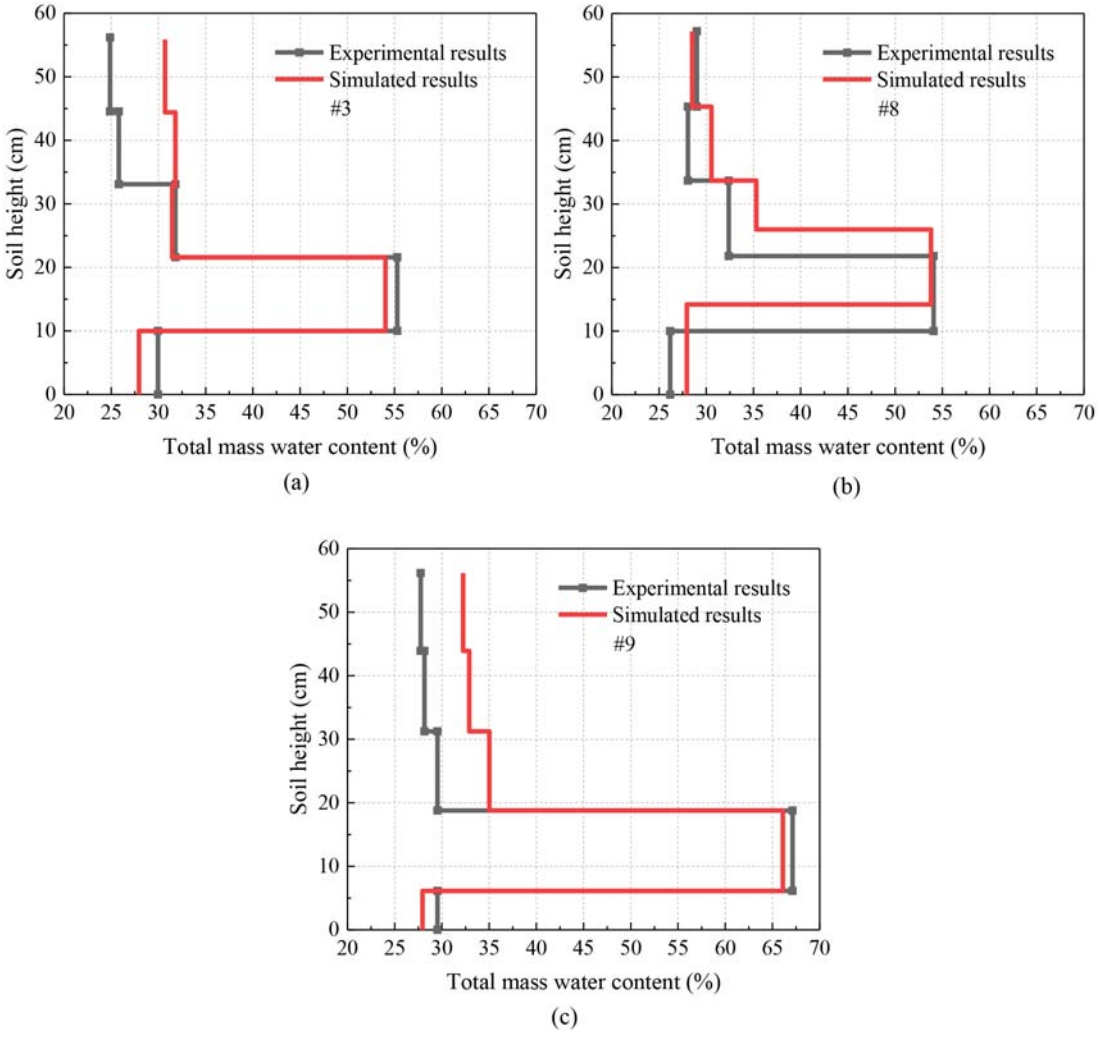

Fig. 8. Comparison between the Experimental and Calculated Total Mass Water Contents after Freezing for 20 h under Different Temperature Gradients: (a) #3, (b) #8, (c) #9

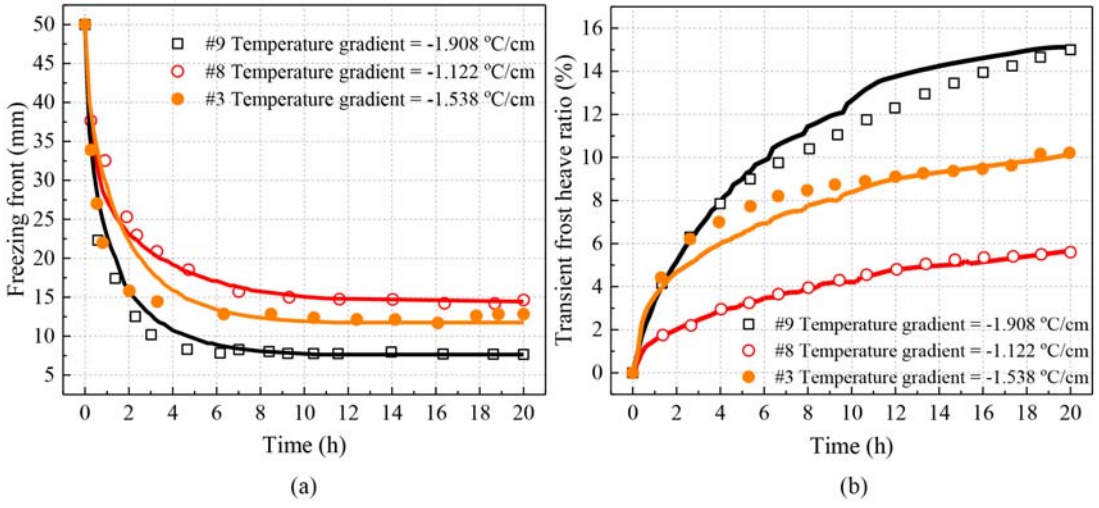

Fig. 9. Dynamic Variation in the Freezing Front and Frost Heave Ratio under Different Temperature Gradients (Symbol: Experimental Results; Line: Calculated Results): (a) Freezing Front, (b) Frost Heave Ratio

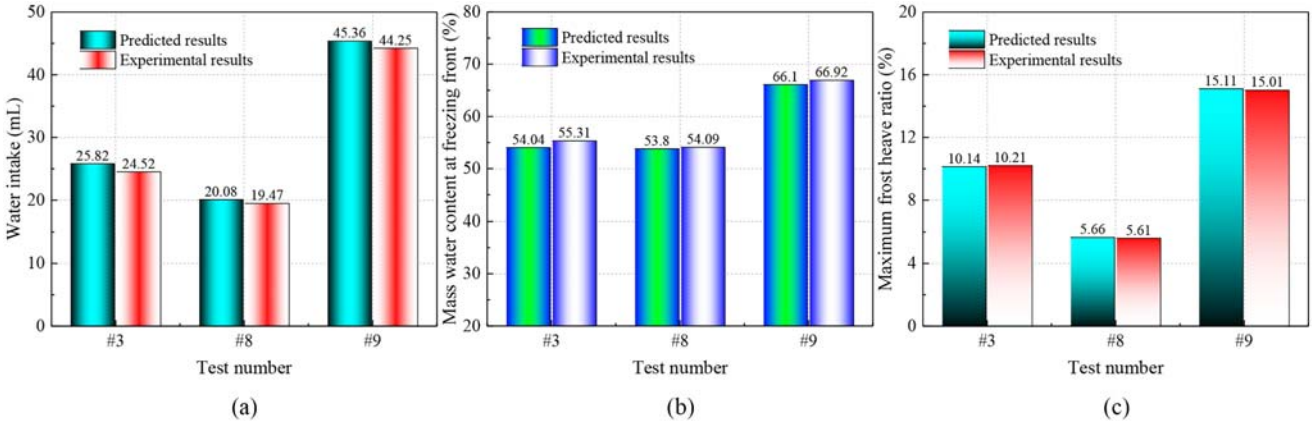

Fig. 10. Comparison between Calculated and Experimental Results under Different Temperature Gradients: (a) Water Intake, (b) Mass Water Content at the Freezing Front, (c) Maximum Frost Heave Ratio

larger the temperature gradient, the larger the frost heave ratio. Moreover, the calculated results of the dynamic variation in the freezing front and frost heave ratio are consistent with the test results.

By comparing the test results of the water intake, mass water content at the freezing front, and maximum frost heave ratio, the calculated results under different temperature gradients are also shown in Fig. 10. The good agreement between the calculated and experimental results confirms the accuracy and feasibility of the simulation with the proposed coupling model.

3.5 Influence of Confining Pressure on Hydro-thermal-mechanical Performance

Figure 11 shows the total mass water content distribution after freezing for 20 h under different confining pressures. The amount of water accumulated near the freezing front decreases with the increase in the confining pressure. This can be explained by the fact that an increase in the confining pressure brings more pores closer and reduces the path of water supply migration, thus affecting the amount of water migration. Moreover, as the temperature at the warm end is only approximately 0.5°C, the depth of the freezing front inside the soil column is closer to the warm end, leading to more water migration and accumulation near the freezing front.

Figure 12 shows a comparison between the experimental and calculated total mass water contents after freezing for 20 h under different confining pressures. Although there is a certain difference between the predicted and experimental results of the water distribution for case #6, the proposed model can predict the water distribution well overall. The difference for case #6 is possibly due to the assumption that the amount of water content in the unfrozen zone remains constant in the model, leading to a deviation in the estimation of the water content near the freezing front. Besides, for case #5, the mass water content reaches 204% near the freezing front. This is because the freezing period of this case #5 is 27 h; therefore, there is sufficient time for more water to migrate.

Figure 13 shows the dynamic variation in the freezing front and frost heave ratio under different confining pressures. The effect of the confining pressure on the development of the freezing front inside the soil column is largely negligible. Besides, with the

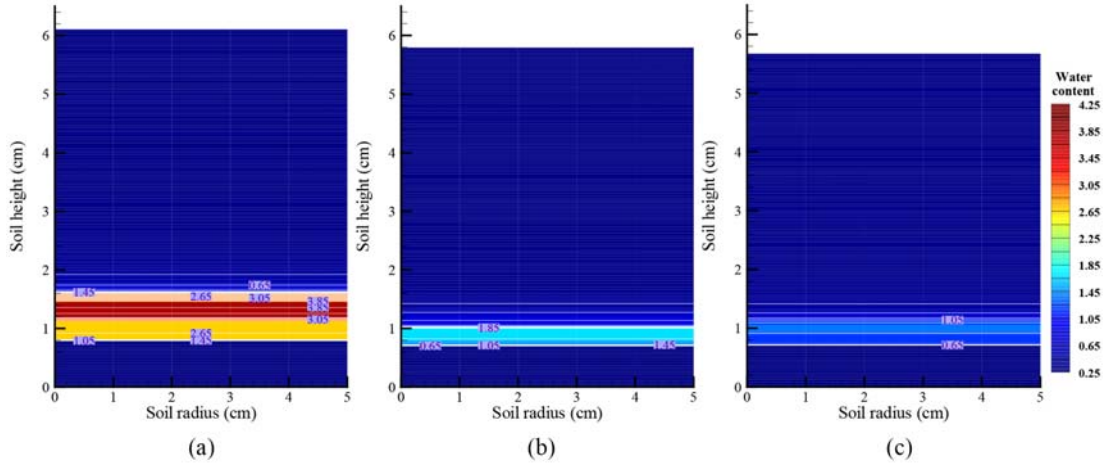

Fig. 11. Total Mass Water Content Distribution after Freezing for 20 h under Different Confining Pressures: (a) #5, (b) #6, (c) #7

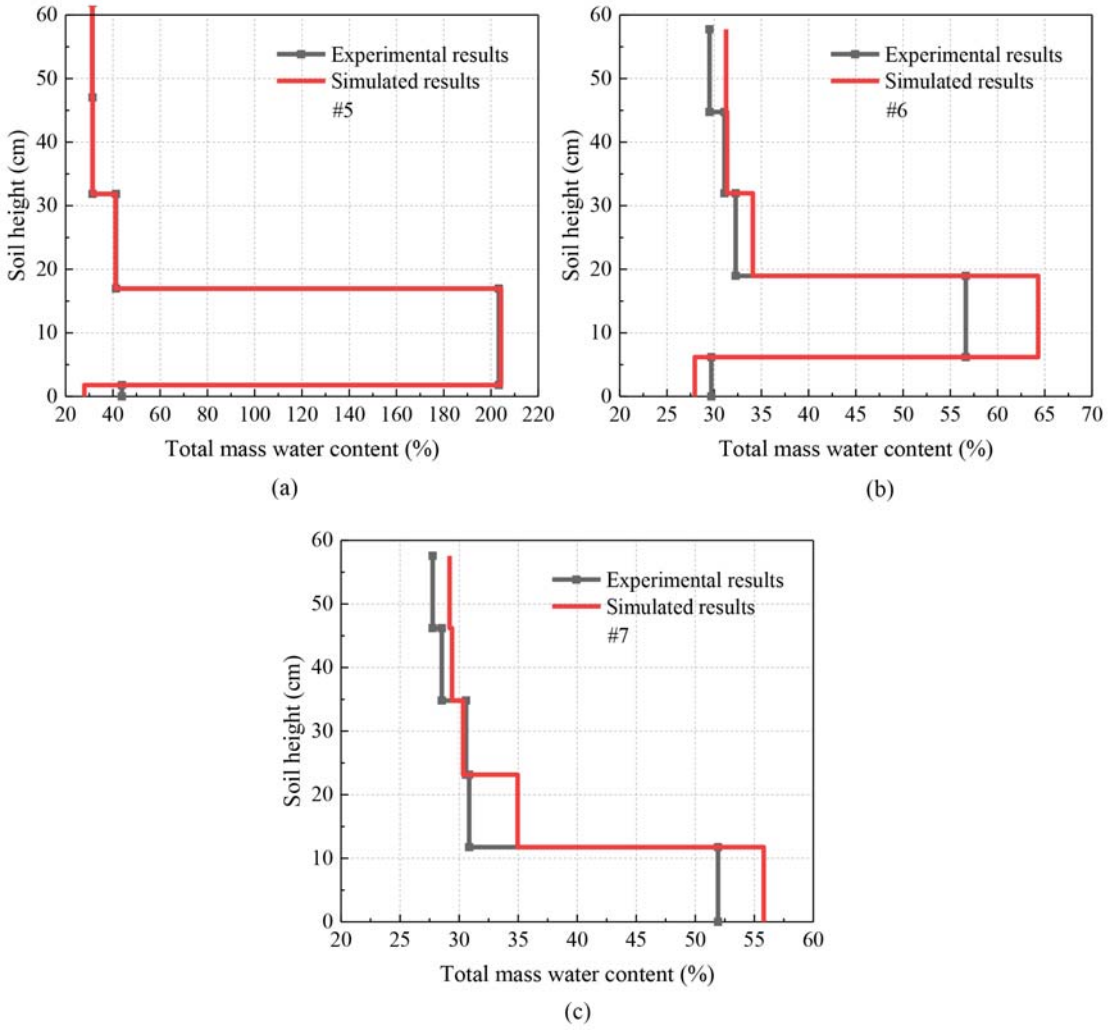

Fig. 12. Comparison between the Experimental and Calculated Total Mass Water Contents after Freezing for 20 h under Different Confining Pressures: (a) #5, (b) #6, (c) #7

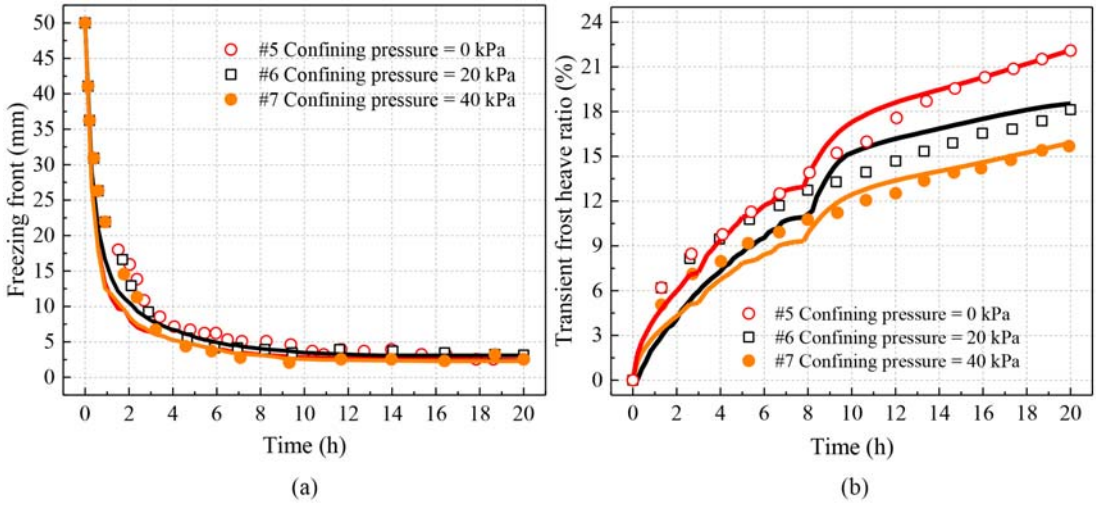

Fig. 13. Dynamic Variations in the Freezing Front and Frost Heave Ratio under Different Confining Pressures (Symbol: Experimental Results; Line: Calculated Results): (a) Freezing Front, (b) Frost Heave Ratio

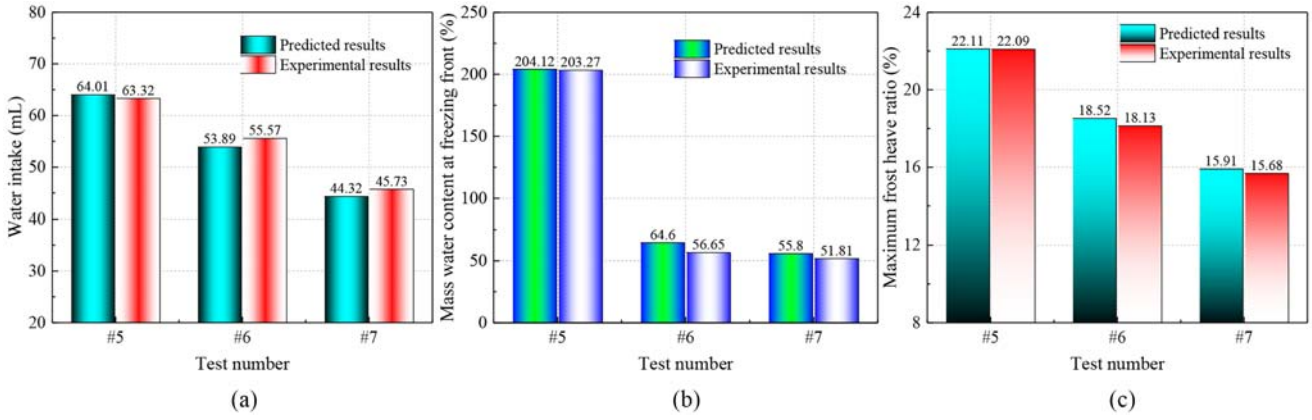

Fig. 14. Comparison between Calculated and Experimental Results under Different Confining Pressures: (a) Water Intake, (b) Mass Water Content at the Freezing Front, (c) Maximum Frost Heave Ratio

increase in the confining pressure, the frost heave ratio also gradually decreases due to the decrease in the water intake. Moreover, the proposed model can be validated directly by comparing the calculated and experimental results under different confining pressures, which can be seen in Fig. 14.

4. Discussion and Limitation

Describing the frost heave, water distribution, and temperature variation in saturated frozen soil under different confining and deviator pressure is very difficult because the anisotropy of frost heave must be considered in the model. Therefore, few coupling models have been proposed up to now. In this study, a heat-water-stress coupling model was established under different stress level, and the calculated results are perfect close to the experimental results by previous studies. However, a limitation of the proposed model is that the soil permeability is determined by the quantity of water intake, not the experiment. Additionally, the anisotropic coefficient is derived from the maximum frost heave in this study because the lateral deformation cannot be obtained from previous studies. Regardless of these limitations, as a preliminary investigation, this study is expected to provide a theoretical basis for engineering applications in cold regions.

5. Conclusions

In this study, a heat-water-stress coupling model for saturated frozen soil under different stress levels was developed to quantify the water redistribution, heat transfer, frost heave, and water intake. The empirical formula for the hydraulic conductivity considering the confining and deviator pressures was employed as an indispensable hydraulic equation in the coupling model. By introducing an anisotropic coefficient, the anisotropic frost heave was further considered in the coupling model. The main conclusions drawn from the analysis are as follows:

1. The developed heat-water-stress coupling model for saturated frozen soil considering the anisotropic frost heave could adequately predict the water redistribution, heat transfer, frost heave, and water intake under different deviator pressures, confining pressures, and temperature gradients.
2. An increase in the deviator and confining pressures will limit the amount of water migration and frost heave ratio; however, their effect on the dynamic variation in the freezing front can be almost negligible. In addition, when the temperature at the warm end is kept constant, the water intake, frost heave ratio, and the depth of the freezing front increases with the increase in the temperature gradient gradually.
3. The hydraulic conductivity could be determined by controlling the calculated water intake close to that in the test. An empirical formula for the hydraulic conductivity considering the confining and deviator pressures was employed, which can be applied to predict the hydraulic conductivity under different test conditions.
4. Based on currently available data, the anisotropic frost heave coefficient was not significantly affected by the deviator pressure. However, the anisotropic frost heave coefficient increased with the increase in the confining pressure and temperature gradient. Unfortunately, because the temperatures at the warm and cold end are difficult to be kept constant in the experiment, it was challenging to propose an accurate prediction formula in this study.

Acknowledgments

This work was supported by the Basic research support program for outstanding young teachers in Heilongjiang provincial universities [Grant Number YQJH2023092], the high-level talent research start-up fund project in Heilongjiang University of Science and Technology [Grant Number HKD202316] and Basic scientific research expenses of Heilongjiang provincial universities [Grant Number 2023-KYYWF-0522].

ORCID

Not Applicable

References

Azmatch TF, Sego DC, Arenson LU, Biggar KW (2012) Using soil freezing characteristic curve to estimate the hydraulic conductivity function of partially frozen soils. *Cold Regions Science and Technology* 83-84:103-109, DOI: 10.1016/j.coldregions.2012.07.002

Bai RQ, Lai YM, Pei WS, Zhang MY (2022) Study on the frost heave behavior of the freezing unsaturated silty clay. *Cold Regions Science and Technology* 197:103525, DOI: 10.1016/j.coldregions.2022.103525

Bai RQ, Lai YM, Zhang MY, Ren JG (2020) Study on the coupled heat-water-vapor-mechanics process of unsaturated soils. *Journal of Hydrology* 585:124784, DOI: 10.1016/j.jhydrol.2020.124784

Cai HB, Cheng Y, Yao ZS (2015) Numerical analysis of ground displacement due to orthotropic frost heave of frozen soil in freezing period of tunnel. *Chinese Journal of Mechanical Engineering* 34(8): 1667-1676, DOI: 10.13722/j.cnki.jrme.2014.0514

Duquennoi C, Fremond M (1989) Modelling of thermal soil behavior. *Valtion Teknillinen Tutkimuskeskus Symposium* 2:895-915

Everett DH (1961) The thermodynamics of frost damage to porous solid. *Transactions Faraday Society* 57:1541-1551, DOI: 10.1039/TF9615701541

Gao JQ, Lai YM, Zhang MY, Feng ZJ (2018) Experimental study on the water-heat-vapor behavior in a freezing coarse-grained soil. *Applied Thermal Engineering* 128:956-965, DOI: 10.1016/j.applthermaleng.2017.09.080

Harlan RL (1973) Analysis of coupled heat-fluid transport in partially frozen soil. *Water Resources Research* 9(5):1314-1323, DOI: 10.1029/WR009i005p01314

Ji YK, Zhou GQ, Vandeginste V, Zhou Y (2021) Thermal-hydraulic-mechanical coupling behavior and frost heave mitigation in freezing soil. *Bulletin of Engineering Geology and the Environment* 80:2701-2713, DOI: 10.1007/s10064-020-02092-3

Konrad JM, Morgenstern NR (1981) The segregation potential of a freezing soil. *Canadian Geotechnical Journal* 18:482-491, DOI: 10.1139/t81-059

Konrad JM, Morgenstern NR (1982) Effects of applied pressure on freezing soils. *Canadian Geotechnical Journal* 19:494-505, DOI: 10.1139/t82-053

Lai YM, Pei WS, Zhang MY, Zhou JZ (2014) Study on theory model of hydro-thermal-mechanical interaction process in saturated freezing silty soil. *International Journal of Heat and Mass Transfer* 78:805-819, DOI: 10.1016/j.ijheatmasstransfer.2014.07.035

Li ZM, Chen J, Tang AP, Sugimoto M (2021) A novel model of heat-water-air-stress coupling in unsaturated frozen soil. *International Journal of Heat and Mass Transfer* 175:121375, DOI: 10.1016/j.ijheatmasstransfer.2021.121375

Li ZM, Chen J, Sugimoto M (2020) Pulsed NMR measurements of unfrozen water content in partially frozen soil. *Journal of Cold Regions Engineering*, 34(3):04020013, DOI: 10.1061/(ASCE)CR.1943-5495.0000220

Li ZM, Chen J, Sun K, Zhang B (2017) Numerical simulation and experimental validation of moisture-heat coupling for saturated frozen soils. *Sciences in Cold and Arid Regions* 9(3):250-257, DOI: 10.3724/SP.J.1226.2017.00250

Li HS, Liu ZL, Li NS (1998) A frost heave model based on moisture temperature and applied load interaction in frozen soil. *Journal of Dalian University Technology* 38(1):29-33

Li SY, Zhang MY, Tian YB, Pei WS, Zhong H (2015) Experimental and numerical investigations on frost damage mechanism of a canal in cold regions. *Cold Regions Science and Technology* 116:1-11, DOI: 10.1016/j.coldregions.2015.03.013

Liu Z, Yu X (2011) Coupled thermo-hydro-mechanical model for porous material under frost action: Theory and implementation. *Acta Geotechnica* 6:51-65, DOI: 10.1007/s11440-011-0135-6

Lu N, (2004) Unsaturated soil mechanics. *John Wiley and Sons*

Lu XF, Zhang F, Qin WJ, Zheng H, Feng, DC (2021) Experimental investigation on frost heave characteristics of saturated clay soil under different stress levels and temperature gradients. *Cold Regions Science and Technology* 192:103379, DOI: 10.1016/j.coldregions.2021.103379

Ming F, Li DQ (2016) A model of migration potential for moisture migration during soil freezing. *Cold Regions Science and Technology* 124:87-94, DOI: 10.1016/j.coldregions.2015.12.015

Mualem Y (1976) A new model for predicting the hydraulic conductivity of unsaturated porous media. *Water Resource Research* 12(3):513-522, DOI: 10.1029/WR012i003p00513

O'neill K, Miller RD (1985) Exploration of a rigid ice model of frost heave. *Water Resource Research* 21(3):281-296, DOI: 10.1029/WR021i003p00281

Qu DX, Luo Y, Li XP, Wang G, Zhang G, Xu K (2020) Study on the stability of rock slope under the coupling of stress field, seepage field, temperature field, and chemical field. *Arabian Journal for Science and Engineering* 45:8315-8329, DOI: 10.1007/s13369-020-04723-z

She W, Cao X, Zhao G, Cai DG, Jiang JY (2018) Experimental and numerical investigation of the effect of soil type and fineness on soil frost heave behavior. *Cold Regions Science and Technology* 148:148-158, DOI: 10.1016/j.coldregions.2018.01.015

Shen M, Branko L (1987) Modeling of coupled heat moisture and stress field in freezing soil. *Cold Regions Science and Technology* 14:237-246, DOI: 10.1016/0165-232X(87)90016-4

Shen Y, Tang T, Zuo R, Tian YH, Zhang ZQ, Wang YQ (2020) The effect and parameter analysis of stress release holes on decreasing frost heaves in seasonal frost areas. *Cold Regions Science and Technology* 169:102898, DOI: 10.1016/j.coldregions.2019.102898

Taber S (1929) Frost heaving. *Journal of Geology* 37:428-461, DOI: 10.1086/623637

Taber S (1930) The mechanics of frost heaving. *Journal of Geology* 38:303-317, DOI: 10.1086/623720

Tan XJ, Chen WZ, Tian HM, Gao JJ (2011) Water flow and heat transport including ice/water phase change in porous media: Numerical simulation and application. *Cold Regions Science and Technology* 68:74-84, DOI: 10.1016/j.coldregions.2011.04.004

Teng JD, Liu JL, Zhang S, Sheng DC (2020) Modelling frost heave in unsaturated coarse-grained soils. *Acta Geotechnica* 15:3307-3320, DOI: 10.1007/s11440-020-00956-2

Wu DY, Lai YM, Zhang MY (2017) Thermo-hydro-salt-mechanical coupled model for saturated porous media based on crystallization kinetics. *Cold Regions Science and Technology* 133:94-107, DOI: 10.1016/j.coldregions.2016.10.012

Xue K, Wen Z, Zhu ZY, Wang DY, Luo F, Zhang ML (2021) An experimental study of the relationship between the matric potential, unfrozen water, and segregated ice of saturated freezing soil. *Bulletin of Engineering Geology and the Environment* 80:2535-2544, DOI: 10.1007/s10064-020-02052-x

Yin X, Liu EL, Song BT, Zhang D (2018) Numerical analysis of coupled liquid water, vapor, stress, and heat transport in unsaturated freezing soil. *Cold Regions Science and Technology* 155:20-28, DOI: 10.1016/j.coldregions.2018.07.008

Yu LY, Zeng YJ, Wen J, Su ZB (2018) Liquid-vapor-air flow in the frozen soil. *Journal of Geophysical Research: Atmospheres* 123: 7393-7415, DOI: 10.1029/2018JD028502

Yuan RH, Bai J, Wu GF (2012) Test study on soil-cement permeability coefficient change with confining pressure of a flexible wall permeameter. *Journal of Hydrologic Engineering* 5:13-17, DOI: 10.16198/j.cnki.1009-640x.2012.05.010

Zhang ZY, Yu QH, Wang JG, Pan Y, Liu EL, Wang XB (2021) Heat transfer characteristics of gravelly soils with different compactness during unidirectional freezing process. *Heat and Mass Transfer* 57:1161-1170, DOI: 10.1007/s00231-021-03022-z

Zhang XY, Zhang MY, Lu JG, Pei WS, Yan ZR (2017a) Effect of hydro-thermal behavior on the frost heave of a saturated silty clay under different applied pressures. *Applied Thermal Engineering* 117:462-467, DOI: 10.1016/j.applthermaleng.2017.02.069

Zhang MY, Zhang XY, Li SY, Lu JG (2017b) Effect of temperature gradients on the frost heave of a saturated silty clay with a water supply. *Journal of Cold Regions Engineering* 31:1-11, DOI: 10.1061/(ASCE)CR.1943-5495.0000137

Zhang XY, Zhang MY, Pei WS, Lu JG (2018) Experimental study of the hydro-thermal characteristics and frost heave behavior of a saturated silt within a closed freezing system. *Applied Thermal Engineering* 129:1447-1454, DOI: 10.1016/j.applthermaleng.2017.10.116

Zhao XD, Li T, Ji YK (2021) Experimental study on 2D freezing in saturated soils. *Journal of Cold Regions Engineering* 35(2):06021002, DOI: 10.1061/(ASCE)CR.1943-5495.0000248

Zhou JZ, Li DQ (2012) Numerical analysis of coupled water, heat, stress in unsaturated freezing soil. *Cold Regions Science and Technology* 157:215-223, DOI: 10.1016/j.coldregions.2011.11.006

Zhou ZW, Ma W, Zhang SJ, Mu YH, Li GY (2020) Experimental investigation of the path dependent strength and deformation behaviors of frozen loess. *Engineering Geology* 265:105449, DOI: 10.1016/j.enggeo.2019.105449

Appendix: Parameters of the Model

A1. Hydraulic Characteristics:

The permeability of the frozen soil k can be expressed as (Mualem, 1976):

$$k = k_y' k_r = k_y' S_l^p \left(1-\left(1-S_l^{1/m}\right)^m\right)^2 \tag{27}$$

where k_r is the relative permeability; S_l is the effective saturation; p and m are the fitting parameters, which are equal to 0.5 and 0.26, respectively.

The specific water capacity C_φ can be expressed as (Li et al., 2017):

$$C_\varphi = a_0 m/(1-m) S_l^{1/m} \left(1-S_l^{1/m}\right)^m \tag{28}$$

where a_0 is the fitting parameter related to the property of the soil and is equal to 2.65 in this study.

A2. Mechanical Characteristics:

The elastic matrix $[D_T]$ that depends on the temperature can be expressed as (Li et al., 2015):

$$[D_T] = \frac{E_T(1-\nu_T)}{(1+\nu_T)(1-2\nu_T)} \begin{bmatrix} 1 & \frac{\nu_T}{1-\nu_T} & 0 \\ \frac{\nu_T}{1-\nu_T} & 1 & 0 \\ 0 & 0 & \frac{1-2\nu_T}{2(1-\nu_T)} \end{bmatrix} \tag{29}$$

where E_T (MPa) and ν_T are the elastic modulus and Poisson's ratio, respectively. The two variables are both relative to the temperature, expressed as (Zhou et al., 2020):

$$E_T = \begin{cases} c_1 + d_1 (T_f - T)^{f_1} & T \le T_f \\ c_1 & T > T_f \end{cases} \tag{30}$$

$$\nu_T = \begin{cases} c_2 + d_2 (T_f - T)^{f_2} & T \le T_f \\ c_2 & T > T_f \end{cases} \tag{31}$$

where c_1, d_1, f_1, c_2, d_2, and f_2 are the experimental parameters (c_1 = 6; d_1 = 11.3; f_1 = 0.6; c_2 = 0.28; d_2 = -0.007; f_2 = 1).

The Drucker–Prager yield criterion matched with the Mohr–Coulomb criterion was employed in this study, and the yield function can be expressed as:

$$F = \sqrt{J_2} + \alpha I_1 - k_F \tag{32}$$

where I_1 and J_2 are the first stress invariant and second deviatoric stress invariant, respectively. α and k_F denote the material parameters, which can be expressed as a function of the internal friction angle φ_T (°) and cohesion c_T (kPa):

$$\alpha = \frac{2\sin\varphi_T}{\sqrt{3}(3-\sin\varphi_T)} \tag{33}$$

$$k_F = \frac{2\sqrt{3} c_T \cos\varphi_T}{(3-\sin\varphi_T)} \tag{34}$$

The internal friction angle and cohesion can also be expressed as a function of the temperature, as follows:

$$c_T = \begin{cases} c_3 + d_3 (T_f - T)^{f_3} & T \le T_f \\ c_3 & T > T_f \end{cases} \tag{35}$$

$$\varphi_T = \begin{cases} c_4 + d_4 (T_f - T)^{f_4} & T \le T_f \\ c_4 & T > T_f \end{cases} \tag{36}$$

where c_3, d_3, f_3, c_4, d_4, and f_4 are the experimental parameters (c_3 = 20; d_3 = 6; f_3 = 1.24; c_4 = 20; d_4 = 3.4; f_4 = 0.38).